

LagNetViP: A Lagrangian Neural Network for Video Prediction

Christine Allen-Blanchette, Sushant Veer, Anirudha Majumdar, Naomi Ehrich Leonard

Department of Mechanical and Aerospace Engineering, Princeton University
 {ca15, sveer, ani.majumdar, naomi}@princeton.edu

Abstract

The dominant paradigms for video prediction rely on opaque transition models where neither the equations of motion nor the underlying physical quantities of the system are easily inferred. The equations of motion, as defined by Newton’s second law, describe the time evolution of a physical system state and can therefore be applied toward the determination of future system states. In this paper, we introduce a video prediction model where the equations of motion are explicitly constructed from learned representations of the underlying physical quantities. To achieve this, we simultaneously learn a low-dimensional state representation and system Lagrangian. The kinetic and potential energy terms of the Lagrangian are distinctly modelled and the low-dimensional equations of motion are explicitly constructed using the Euler-Lagrange equations. We demonstrate the efficacy of this approach for video prediction on image sequences rendered in modified OpenAI gym Pendulum-v0 and Acrobot environments.

Introduction

Video prediction is a longstanding challenge in computer vision. While neural network models have provided significant advancements in the high-dimensional data regime, these advancements typically fail to provide an interpretable representation of the data-generating distribution. Juxtaposed against increased adoption of neural learning systems in safety critical domains, a growing segment of the community is advocating for the incorporation of physical priors to improve both the interpretability of representations and the generalizability of neural network models (Lake et al. 2017; Higgins et al. 2018). In line with this call, we present a video prediction model that utilizes well-understood physical principles to capture the time evolution of the underlying data-generating process. In video prediction, high-dimensional images represent observations corresponding to low-dimensional states in a dynamical system. This correspondence is captured by the manifold hypothesis, which posits the existence of a low-dimensional manifold for high-dimensional data (Bengio, Courville, and Vincent 2013). By identifying the low-dimensional state-space manifold, well-

Copyright © 2020, Association for the Advancement of Artificial Intelligence (www.aaai.org). All rights reserved.

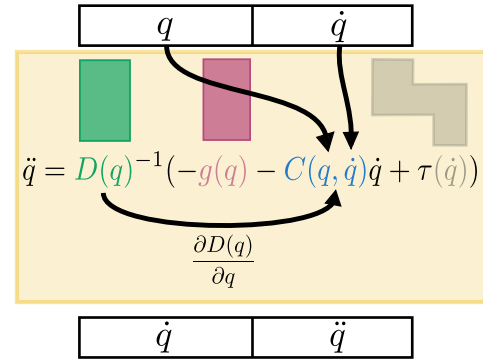


Figure 1: Lagrangian neural network for video prediction (LagNetViP) architecture. LagNetViP (yellow) is comprised of an inertia tensor network (green), potential energy network (purple) and generalized forces network (gray). An auto-encoding network (not shown) can be trained end-to-end with LagNetViP to simultaneously learn a representation of the system state (q, \dot{q}) and the underlying dynamics. The network can also be adapted to settings where the generalized force τ is available as an input.

understood physical principles can be leveraged to model the evolution of the system.

The time evolution of a physical system is determined by its equations of motion. Given the system Lagrangian, which is system kinetic energy minus system potential energy, the equations of motion can be derived using the Euler-Lagrange equations (Goldstein, Poole, and Safko 2002). Previous works (Cranmer et al. 2020; Lutter, Ritter, and Peters 2018) have shown that it is possible to learn the system Lagrangian from low-dimensional measurements. In this work, we present an approach to simultaneously learn a low-dimensional state-space representation and system Lagrangian from high-dimensional image data. In our approach, images are mapped to and from the low-dimensional state-space by an auto-encoding neural network and initial states are integrated forward using the equations of motion determined by the system Lagrangian and Euler-Lagrange equations. Towards interpretability of the representation, the

inertia tensor, which determines the kinetic energy, and the potential energy are parameterized by distinct neural networks. A pictorial representation of our model (LagNetViP) is given in Figure 1.

The efficacy of our approach requires that the auto-encoder and system Lagrangian agree on an appropriate low-dimensional representation. To encourage this, we define the training loss as the sum of three terms: (1) the reconstruction loss of the auto-encoded image sequence, (2) the reconstruction loss of the latent trajectory generated by the learned dynamics and (3) a mean absolute difference between the auto-encoded image sequence and the latent trajectory generated by the learned dynamics. We validate the importance of each term through an ablation study and provide a qualitative assessment using image sequences rendered in modified OpenAI gym `Pendulum-V0` and `Acrobot` environments.

Related work

Recurrent neural networks (RNNs) have been applied to a broad class of sequence prediction problems including language modeling, machine translation, image processing and audio processing (Graves 2013; Cho et al. 2014; Srivastava, Greff, and Schmidhuber 2015; Oord et al. 2016). The utility of RNNs stems from the architectural structure, which enforces parameter sharing and encourages the network to learn statistics that generalize across sequences.

When sequential data can be interpreted as the observations of a dynamical system, the structure of difference or differential equations can be leveraged for prediction. Sequential image data is necessarily discrete although the generating process for image data is continuous. Consequently, there is a disparity in modeling approaches; Watter et al. and Karl et al. model the nature of the data with a (generative) discrete-time dynamical model, while Yildiz, Heinonen, and Lahdesmaki model the continuous generating process with a continuous-time dynamical model. The related work of (Chen et al. 2018) facilitates estimation of continuous-time dynamics with neural networks by allowing for backpropagation through arbitrary ODE solvers.

The structure of the output space of a dynamical system can also be leveraged in learning (Stewart and Ermon 2017). In (Greydanus, Dzamba, and Yosinski 2019; Toth et al. 2019; Bertalan et al. 2019), the authors model the underlying dynamics of sequential data assuming the Hamiltonian structure. Dynamical state updates are generated using Hamilton’s equations. For high-dimensional data, Greydanus, Dzamba, and Yosinski and Toth et al. learn a map from the observation space to a low-dimensional phase space where Hamilton’s equations can be applied. A limitation of these approaches is that they are only applicable in the context of conservative systems. In (Zhong, Dey, and Chakraborty 2019), the authors surpass this limitation by assuming the Port-Hamiltonian structure, which can be used to model nonconservative systems.

In (Lutter, Ritter, and Peters 2018; Cranmer et al. 2020; Saemundsson et al. 2020; Zhong and Leonard 2020), the authors assume the Lagrangian structure which allows for incorporation of nonconservative forces naturally. Saemundsson et al. and Zhong and Leonard introduce generative

models that leverage the variational auto-encoder (VAE) formulation to learn a representation of the low-dimensional state-space from high-dimensional images. Saemundsson et al. use a Gaussian prior on the latent code but set its dimension substantially higher than the number of degrees of freedom inherent to the system. This architectural choice limits interpretability of the learned coordinate representation and may have adverse effects in the control setting. In (Zhong and Leonard 2020) (work concurrent to ours), the authors select the latent dimension according to the number of degrees of freedom in the system. They find that with this choice the standard Gaussian prior severely inhibits learning and instead choose to apply system specific priors on the latent code.

In this work we introduce a discriminative model with latent dimension consistent with the number of degrees of freedom inherent to the system but without the need for system specific structural priors. Other discriminative models that leverage the Lagrangian structure are (Lutter, Ritter, and Peters 2018) and (Cranmer et al. 2020). Our model differs from (Lutter, Ritter, and Peters 2018) in that we learn and apply the *forward* model for dynamical state prediction whereas (Lutter, Ritter, and Peters 2018) learn the *inverse* model for generalized force prediction and control. Moreover, we apply our approach to high-dimensional observations which neither (Lutter, Ritter, and Peters 2018) nor (Cranmer et al. 2020) attempt.

Lagrangian dynamics

In this section, we provide a brief introduction to Lagrangian dynamics. For the sake of brevity, the exposition is kept terse; interested readers can find further details in (Spong and Vidyasagar 2008; Goldstein, Poole, and Safko 2002).

A Lagrangian mechanical system has an associated configuration space \mathcal{Q} which, loosely speaking, includes all the feasible configurations (or poses) q of the mechanical system; e.g., for a simple pendulum, the configuration space can be defined as the space $\mathcal{Q} := [-\pi, \pi)$ of all possible angles. We denote the rate of change of the configuration q by \dot{q} . Mathematically, \mathcal{Q} takes on the structure of a manifold with $q \in \mathcal{Q}$ being a set of coordinates on it and the tuple (q, \dot{q}) lies in its tangent bundle $\mathcal{T}\mathcal{Q}$. The dimension of \mathcal{Q} corresponds to the degrees of freedom of the dynamical system and will be denoted by $m \in \mathbb{N}$ throughout the paper.

The Lagrangian $L : \mathcal{T}\mathcal{Q} \rightarrow \mathbb{R}$ is a function that maps the tangent space $\mathcal{T}\mathcal{Q}$ to a scalar. To define the Lagrangian first requires the introduction of the kinetic energy $T : \mathcal{T}\mathcal{Q} \rightarrow [0, \infty)$ and the potential energy $V : \mathcal{Q} \rightarrow \mathbb{R}$. Intuitively, the kinetic energy T is the energy possessed by a mechanical system by virtue of its motion whereas the potential energy V is the energy stored in a mechanical system due to its configuration. We assume the form of the kinetic energy to be quadratic in the velocity, as follows:

$$T = \frac{1}{2} \dot{q}^T D(q) \dot{q} \quad (1)$$

where $D : \mathcal{Q} \rightarrow \mathbb{S}_{++}^n$ is the positive definite inertia matrix. The kinetic energy of any mechanical system with holonomic constraints satisfies the quadratic form (1) — see

(Spong and Vidyasagar 2008) for examples. Hence, learning the quadratic form (1) allows us to embed more structure in our architecture without compromising the richness of the class of systems that can be addressed by our approach. Indeed, the quadratic form of the kinetic energy has also been adopted in SymODEN (Zhong, Dey, and Chakraborty 2019) and DeLaN (Lutter, Ritter, and Peters 2018). With the kinetic and the potential energy introduced above, we can express the Lagrangian L as the difference between them:

$$L(q, \dot{q}) = T(q, \dot{q}) - V(q). \quad (2)$$

The equations of motion for the Lagrangian dynamical system can be conveniently uncovered by the following operation on the Lagrangian (Euler-Lagrange equations):

$$\frac{d}{dt} \frac{\partial L}{\partial \dot{q}} - \frac{\partial L}{\partial q} = \tau \quad (3)$$

where τ represents the generalized forces, which encapsulate the effect of exogenous influences on the evolution of the Lagrangian system. For systems for which the total energy is conserved, $\tau = 0$. However, the explicit presence of τ in our Lagrangian formalism allows us to handle non-conservative influences with ease, e.g., friction in the pendulum system.

The equations of motion (3) can be expanded further by using (1) and (2) in (3) giving:

$$D(q)\ddot{q} + C(q, \dot{q}) + g(q) = \tau, \quad (4)$$

where $D(q)$ is the inertia matrix, $C(q, \dot{q})$ is the Coriolis term, $g(q) := \frac{\partial V(q)}{\partial q}$, and τ are the generalized forces.

Noting that $D(q)$ is positive definite, we can solve for the acceleration \ddot{q} :

$$\ddot{q} = -D(q)^{-1} \left(C(q, \dot{q}) + g(q) - \tau \right). \quad (5)$$

The Lagrangian dynamics admit further structure that allows us to express the components of the Coriolis term C as a function of the components of the inertia matrix D . For any $k \in \{1, 2, \dots, m\}$, we can express the k -th row of C , denoted by $C_k(q, \dot{q})$, as $C_k(q, \dot{q}) = \sum_{i,j} c_{ijk} \dot{q}_i \dot{q}_j$. Further, the terms c_{ijk} take the form (Spong and Vidyasagar 2008):

$$c_{ijk} = \left\{ \frac{\partial d_{k,j}}{\partial q_i} - \frac{1}{2} \frac{\partial d_{ij}}{\partial q_k} \right\}.$$

Lagrangian neural networks

In this section, we review estimation of the system Lagrangian in the context of low-dimensional state-space measurements and introduce a strategy for estimating the system Lagrangian from (high-dimensional) image data.

Learning from state-space measurements

We outline first our approach for estimating the system Lagrangian from low-dimensional position-velocity measurements. The system Lagrangian is modelled as the difference between the kinetic and potential energies where the mass

matrix D_θ and potential energy function V_ϕ are parameterized by neural networks

$$L(q, \dot{q}) = \frac{1}{2} \dot{q}^T D_\theta(q) \dot{q} - V_\phi(q).$$

This formulation differs from previous work (Cranmer et al. 2020) where neither the kinetic energy nor the potential energy are explicitly modelled and from (Lutter, Ritter, and Peters 2018) where the potential force is modelled instead of the potential energy. To ensure invertibility of the mass matrix D_θ we use an intermediate matrix J_θ of the same shape and compute D_θ by

$$D_\theta(q) = J_\theta(q)^T J_\theta(q) + \lambda I.$$

In our experiments λ is set to the dimension of the position vector q .

The parameters (θ, ϕ) of the system Lagrangian are estimated by iterative minimization of the mean absolute difference between ground truth position-velocity measurement sequences denoted $Z_n = \{z_1^n, \dots, z_T^n\}$, with $z_t^n = (q_t^n, \dot{q}_t^n)$ and $n \in \{1, \dots, N\}$, and predicted sequences \hat{Z}_n defined similarly. The minimization problem is given by

$$(\theta^*, \phi^*) = \arg \min_{\theta, \phi} \frac{1}{N} \sum_{n,t} |z_t^n - \hat{z}_t^n| \quad t \in \{1, \dots, T\}. \quad (6)$$

Predicted sequences are computed recursively from an initial ground truth measurement z_0^n and the current values of θ and ϕ . Concretely, the predicted measurement \hat{z}_{t+1}^n is computed from the preceding measurement \hat{z}_t^n with $\hat{z}_n^0 := z_n^0$ and the dynamical update \hat{z}_t^n given by

$$\hat{z}_t^n = \left(\dot{q}_t^n, -D_\theta(q_t^n)^{-1} \left(C_\theta(q_t^n, \dot{q}_t^n) + g_\phi(q_t^n) - \tau \right) \right).$$

The Coriolis term C_θ and potential force g_ϕ are discussed in the previous section. In our experiments we consider systems without external forces, that is $\tau = 0$, and perform numerical integration with the Euler method. Note that the use of more sophisticated numerical integrators, in particular variational integrators, would likely improve performance.

Learning from image sequences

In this section we outline our approach for estimating the state-space representation and system Lagrangian from high-dimensional observations¹. Our prediction pipeline maps high-dimensional observations to a low-dimensional state-space representation whose structure is learned during the training phase. We predict future low-dimensional states using the Euler-Lagrange equations, then map the resulting sequence back to the observation space giving the predicted image sequence.

To compress and reconstruct observations of system trajectories given as temporal sequences of T high-dimensional observations $X_n = \{x_0^n, \dots, x_T^n\}$, with $n \in \{0, \dots, N\}$, we use an auto-encoding neural network $f = D_\phi \circ E_\phi$, where D_ϕ and E_ϕ are decoding and encoding networks

¹Since we cannot perform velocity prediction from a single image we use observations which we define as image tuples.

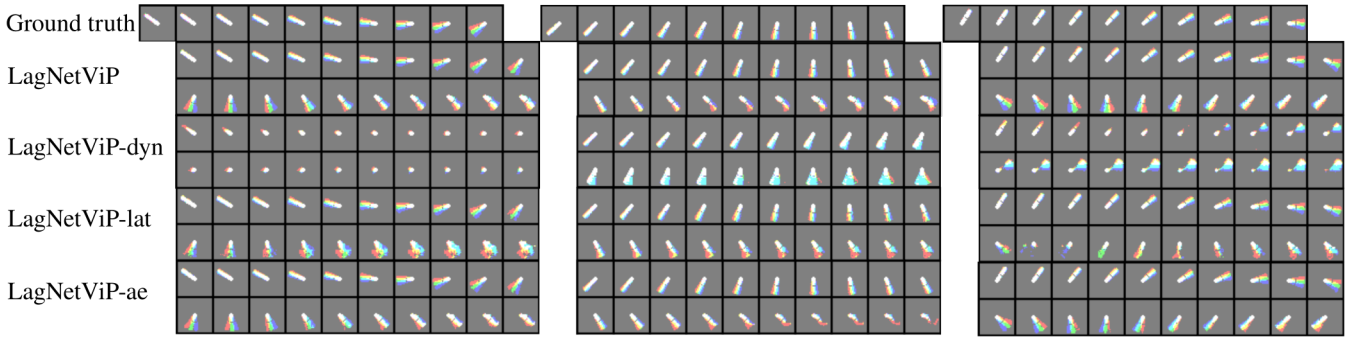


Figure 2: Ablative analysis of the LagNetViP loss function on the pendulum dataset. Top to bottom, (1) Three randomly selected testset trajectories, (2) LagNetViP generated trajectory (two rows), (3) LagNetViP-dyn generated trajectory (two rows), (4) LagNetViP-lat generated trajectory (two rows), (5) LagNetViP-ae generated trajectory (two rows). The testset trajectories for the pendulum dataset consist of 10 observations (over time). To demonstrate how well the dynamics are learned, the first observation of each testset trajectory is encoded to the low-dimensional state-space and integrated forward 20 steps (over time) according to the learned dynamics model. This trajectory is reconstructed giving the image sequences show in the figure. Consider LagNetViP in the left most panel. The first row (frames 1-10) illustrates how well the model extrapolates within the range of the testset and the second row (frames 11-20) illustrates how well the model can extrapolate (forward in time) beyond the range of the testset.

respectively. We denote encoded observation sequences $Z_n = \{z_1^n, \dots, z_T^n\}$ and interpret $z_t^n = E_\phi(x_t^n)$ as a position-velocity measurement. Predicted sequences $\hat{Z}_n = \{\hat{z}_1^n, \dots, \hat{z}_T^n\}$ are determined as described in the previous section.

The parameters (φ, ϕ) of the auto-encoding network and (θ, ψ) of the system Lagrangian are estimated jointly by iterative minimization of the three component loss function:

$$\mathcal{L}_{total} = \mathcal{L}_{ae} + \mathcal{L}_{dyn} + \gamma \mathcal{L}_{lat},$$

where \mathcal{L}_{ae} is the auto-encoding reconstruction loss:

$$\mathcal{L}_{ae}(\mathbf{X}) = \frac{1}{NT} \sum_{n=0}^N \sum_{t=0}^{T-1} \|x_t^n - f(x_t^n)\|_2^2,$$

with $\mathbf{X} = \{X_0, \dots, X_N\}$; \mathcal{L}_{dyn} is the predicted sequence reconstruction loss:

$$\mathcal{L}_{dyn}(\mathbf{X}) = \frac{1}{NT} \sum_{n=0}^N \sum_{t=1}^T \|D_\varphi(\hat{z}_t^n) - x_t^n\|_2^2;$$

and \mathcal{L}_{lat} is the distance between encoded and predicted sequences:

$$\mathcal{L}_{lat}(\mathbf{X}) = \frac{1}{N} \sum_{n=1}^N \sum_{t=0}^T \|\hat{z}_t^n - E_\phi(x_t^n)\|_2^2.$$

This formulation differs from previous work (Greydanus, Dzamba, and Yosinski 2019) where a structural prior is imposed on the embedding space. In our experiments we set $\gamma = 0.1$.

Empirical analysis

In this section we empirically validate the proposed approach. Toward this end, we perform an ablation study

where components of the cost function are removed and a qualitative comparison of the results are presented. Specifically, we compare the following models:

1. LagNetViP: The proposed model that simultaneously learns a low-dimensional state-space representation and system Lagrangian from high-dimensional image data. The training loss is the sum of three terms: (1) the auto-encoder reconstruction loss, (2) the reconstruction loss of the latent trajectory generated by the learned dynamics and (3) a mean absolute difference between the auto-encoded image sequence and the latent trajectory generated by the learned dynamics.
2. LagNetViP-dyn: The proposed model trained without a reconstruction loss on the latent trajectory generated by the learned dynamics.
3. LagNetViP-lat: The proposed model trained without a mean absolute difference between the auto-encoded image sequence and the latent trajectory generated by the learned dynamics.
4. LagNetViP-ae: The proposed model trained without the auto-encoder reconstruction loss.

In each model, we use a symmetric auto-encoding network to map high-dimensional observations to a low-dimensional state-space representation. The encoding network is a four layer neural network: three convolutional layers followed by a fully-connected layer (see Table 1); where convolutional layer is followed by a ReLU nonlinear unit. Both the inertia tensor and potential energy functions are parameterized by three layer fully-connected neural networks with 200 hidden units in each layer and \tanh nonlinear units.

To demonstrate the efficacy of our approach on video prediction problems, we consider image sequences generated using modified OpenAI gym Pendulum-V0 and

Table 1: Encoder configuration. Filter column: (Layers 1-3) width, height, channel and output dimension of convolutional filters; (Layer 4P) the input and output dimension of the fully-connected layer for the pendulum experiment; (Layer 4A) the input and output dimension of the fully-connected layer for the Acrobot experiment.

Layer	Filter	Stride	Padding
1	4x4x3x12	2	1
2	4x4x12x24	2	1
3	4x4x24x12	2	1
4P	(4*4*12)x4	2	1
4A	(4*4*12)x6	2	1

Acrobot environments. To generate image sequences we modify the OpenAI gym environments to use RK4 integration instead of Euler integration and increase the width of the pendulum and Acrobot arms in rendering.

Pendulum Dataset. The pendulum dataset consists of $N = 10,000$ trajectories. Each trajectory is comprised of $T = 10$ observations and each observation is constructed by concatenating three sequential images along the channel dimension. We train on 8,000 of the 10,000 trajectories using the Adam optimizer (Kingma and Ba 2014) with a learning rate of 1×10^{-3} and weight decay of 1×10^{-5} .

Acrobot. The Acrobot dataset consists of $N = 10,000$ trajectories. Each trajectory is comprised of $T = 2$ observations and each observation is constructed by concatenating three sequential images along the channel dimension. We train on 8,000 of the 10,000 trajectories using the Adam optimizer (Kingma and Ba 2014) with a learning rate of 1×10^{-4} and weight decay of 1×10^{-5} .

Results

Figures 2 and 3 present qualitative comparisons on randomly selected testset trajectories from the pendulum and Acrobot datasets. On both datasets LagNetViP is able to extrapolate beyond the last observation in the testset trajectory. Removing the reconstruction loss on the latent trajectory generated by the learned dynamics has the most disastrous effect on reconstruction quality. This is evident in the fact that LagNetViP-dyn is unable to provide reasonable reconstructions even within the range of the testset in some cases. LagNetViP-lat performs well within the testset range but is unable to extrapolate farther and LagNetViP-ae exhibits good performance but fails to out perform LagNetViP.

Consider the trajectory generated by the LagNetViP model in the left-most panel of Figure 2. The position of the pendulum begins pointing up and to the left of the fixed point. In the first 10 frames, the pendulum swings down but not quite reaching the downward pointing position, as in the trajectory of the testset. LagNetViP is able to extrapolate beyond the testset trajectory predicting the upward swing of the pendulum on the right side through the downward pointing position.

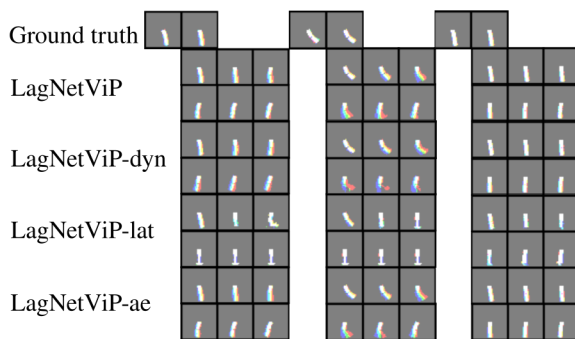


Figure 3: Ablative analysis of the LagNetViP loss function on the Acrobot dataset. Top to bottom. (1) Three randomly selected testset trajectories, (2) LagNetViP generated trajectory (two rows), (3) LagNetViP-dyn generated trajectory (two rows), (4) LagNetViP-lat generated trajectory (two rows), (5) LagNetViP-ae generated trajectory (two rows). The testset trajectories for the pendulum dataset consist of 2 observations (over time). To demonstrate how well the dynamics are learned, the first observation of each testset trajectory is encoded to the low-dimensional state-space and integrated forward 6 steps (over time) according to the learned dynamics model. This trajectory is reconstructed giving the image sequences show in the figure. Consider LagNetViP in the left most panel. The first row (frames 1-3) illustrates how well the model extrapolates within the range of the testset and the second row (frames 4-6) illustrates how well the model can extrapolate (forward in time) beyond the range of the testset.

Discussion and Conclusion

In this work, we introduce a video prediction model where equations of motion are explicitly constructed from learned representations of underlying physical quantities. The low-dimensional state-space representation and system Lagrangian are learned simultaneously. Images are mapped to and from the low-dimensional state-space by an auto-encoding network and initial states are integrated forward using the equations of motion determined by the system Lagrangian and Euler-Lagrange equations. The approach excels over the baseline model with strong reconstruction performance on the pendulum system and strong indications of possibility on the chaotic Acrobot system.

Acknowledgements

We thank Shinkyu Park, Desmond Zhong, David Isele and Patricia Posey for their insights. This research has been supported in part by ONR grant #N00014-18-1-2873 and by the School of Engineering and Applied Science at Princeton University through the generosity of William Addy '82.

References

- [Bengio, Courville, and Vincent 2013] Bengio, Y.; Courville, A.; and Vincent, P. 2013. Representation learning: A review and new perspectives. *IEEE Trans-*

actions on Pattern Analysis and Machine Intelligence 35(8):1798–1828.

- [Bertalan et al. 2019] Bertalan, T.; Dietrich, F.; Mezić, I.; and Kevrekidis, I. G. 2019. On learning Hamiltonian systems from data. *Chaos: An Interdisciplinary Journal of Nonlinear Science* 29(12):121107.
- [Chen et al. 2018] Chen, T. Q.; Rubanova, Y.; Bettencourt, J.; and Duvenaud, D. K. 2018. Neural ordinary differential equations. In *Advances in Neural Information Processing Systems*, 6571–6583.
- [Cho et al. 2014] Cho, K.; van Merriënboer, B.; Gülçehre, Ç.; Bahdanau, D.; Bougares, F.; Schwenk, H.; and Bengio, Y. 2014. Learning phrase representations using RNN encoder-decoder for statistical machine translation. In *Proceedings of the 2014 Conference on Empirical Methods in Natural Language Processing*, 1724–1734. ACL.
- [Cranmer et al. 2020] Cranmer, M.; Greydanus, S.; Hoyer, S.; Battaglia, P.; Spergel, D.; and Ho, S. 2020. Lagrangian neural networks. In *ICLR 2020 Workshop on Integration of Deep Neural Models and Differential Equations*.
- [Goldstein, Poole, and Safko 2002] Goldstein, H.; Poole, C. P.; and Safko, J. L. 2002. *Classical Mechanics Third Edition*. Pearson Education, Inc, publishing as Addison Wesley.
- [Graves 2013] Graves, A. 2013. Generating sequences with recurrent neural networks. *arXiv preprint arXiv:1308.0850*.
- [Greydanus, Dzamba, and Yosinski 2019] Greydanus, S.; Dzamba, M.; and Yosinski, J. 2019. Hamiltonian neural networks. In *Advances in Neural Information Processing Systems*, 15379–15389.
- [Higgins et al. 2018] Higgins, I.; Amos, D.; Pfau, D.; Racaniere, S.; Matthey, L.; Rezende, D.; and Lerchner, A. 2018. Towards a definition of disentangled representations. *arXiv preprint arXiv:1812.02230*.
- [Karl et al. 2017] Karl, M.; Soelch, M.; Bayer, J.; and van der Smagt, P. 2017. Deep variational Bayes filters: Unsupervised learning of state space models from raw data. In *International Conference on Learning Representations*.
- [Kingma and Ba 2014] Kingma, D. P., and Ba, J. 2014. Adam: A method for stochastic optimization. *arXiv preprint arXiv:1412.6980*.
- [Lake et al. 2017] Lake, B. M.; Ullman, T. D.; Tenenbaum, J. B.; and Gershman, S. J. 2017. Building machines that learn and think like people. *Behavioral and Brain Sciences* 40.
- [Lutter, Ritter, and Peters 2018] Lutter, M.; Ritter, C.; and Peters, J. 2018. Deep Lagrangian networks: Using physics as model prior for deep learning. In *International Conference on Learning Representations*.
- [Oord et al. 2016] Oord, A. v. d.; Dieleman, S.; Zen, H.; Simonyan, K.; Vinyals, O.; Graves, A.; Kalchbrenner, N.; Senior, A.; and Kavukcuoglu, K. 2016. WaveNet: A generative model for raw audio. *arXiv preprint arXiv:1609.03499*.
- [Saemundsson et al. 2020] Saemundsson, S.; Terenin, A.; Hofmann, K.; and Deisenroth, M. 2020. Variational integrator networks for physically structured embeddings. *Proceedings of Machine Learning Research*.
- [Spong and Vidyasagar 2008] Spong, M. W., and Vidyasagar, M. 2008. *Robot Dynamics and Control*. John Wiley & Sons.
- [Srivastava, Greff, and Schmidhuber 2015] Srivastava, R. K.; Greff, K.; and Schmidhuber, J. 2015. Highway networks. *arXiv preprint arXiv:1505.00387*.
- [Stewart and Ermon 2017] Stewart, R., and Ermon, S. 2017. Label-free supervision of neural networks with physics and domain knowledge. In *Thirty-First AAAI Conference on Artificial Intelligence*.
- [Toth et al. 2019] Toth, P.; Rezende, D. J.; Jaegle, A.; Racanière, S.; Botev, A.; and Higgins, I. 2019. Hamiltonian generative networks. In *International Conference on Learning Representations*.
- [Watter et al. 2015] Watter, M.; Springenberg, J.; Boedecker, J.; and Riedmiller, M. 2015. Embed to control: A locally linear latent dynamics model for control from raw images. In *Advances in Neural Information Processing Systems* 28. 2746–2754.
- [Yildiz, Heinonen, and Lahdesmaki 2019] Yildiz, C.; Heinonen, M.; and Lahdesmaki, H. 2019. ODE2VAE: Deep generative second order ODEs with bayesian neural networks. In *Advances in Neural Information Processing Systems* 32. 13412–13421.
- [Zhong and Leonard 2020] Zhong, Y. D., and Leonard, N. E. 2020. Unsupervised learning of Lagrangian dynamics from images for prediction and control. In *Advances in Neural Information Processing Systems*.
- [Zhong, Dey, and Chakraborty 2019] Zhong, Y. D.; Dey, B.; and Chakraborty, A. 2019. Symplectic ODE-net: Learning Hamiltonian dynamics with control. In *International Conference on Learning Representations*.